JOURNAL OF MATERIALS SCIENCE 25 (1990) 5081–5090

Compressional behaviour of carbon fibres

Part 1 *A Raman spectroscopic study*

N. MELANITIS, C. GALIOTIS*
Department of Materials, Queen Mary and Westfield College, Mile End Road, London E1 4NS, UK

The axial compressive strain to failure of various types of PAN-based carbon fibres was measured by applying small and defined compressive loads to single filaments which have been bonded to a rectangular polymer cantilever beam and parallel to its long edge. By monitoring the Raman frequencies along the fibre with the 2 μm laser probe of a Raman microscope, the critical compressive strain required for first fibre failure could be assessed and the residual load that each type of fibre supported after first failure, could be measured. Estimates of the compressive moduli for all fibres could, also, be obtained by considering the dependence of the Raman frequency upon compressive strain in the elastic region. The critical compressive strain to failure was found to decrease with fibre modulus and its value was, approximately, equal to 50% of the tensile fracture strain. However, for some low-modulus fibres the compressive strain to failure was found to approach the tensile fracture strain. The initial compressive moduli of high-modulus fibres were estimated to decrease up to a maximum of 10% with respect to their tensile moduli, whereas more significant reductions were found in the case of intermediate and low-modulus fibres.

1. Introduction

A variety of methods have been employed to date, in an attempt to measure the axial compressive strength of high-performance fibres. The most commonly used method is the elastica loop test originated by Sinclair [1]; a loop is induced in a fibre which is trapped in an oil immersion between two microscope slides and, then, by pulling the two ends of the fibre, the loop is reduced gradually in size. An examination of the photographs at each stage of the loop provides useful information on the level of tensile or compressive stresses developed at the outer or inner surfaces of the fibre, respectively. In theory, the ratio of major to minor axis should stay constant and equal to 1.34, as long as the fibre behaves elastically [2]. Any deviation from that value would indicate that some form of non-Hookean behaviour takes place. The strain, ε, at any point in the loop is given by

$$\varepsilon = \frac{r}{R} \tag{1}$$

where r is the radius of the fibre and R the radius of the curvature. Hence, for thin fibres, very small radii of curvature are required to obtain strains high enough to fail the specimen.

The elastica loop method has been used to measure the intrinsic compressive strain to failure of Kevlar 49 fibres, 12 μm diameter, although the values reported were surprisingly high [3]. However, the applicability of the elastica loop test on carbon fibres is problematic for the following reasons: (a) commercial carbon fibres are difficult to handle due to their small sizes, typically 5 to 7 μm in diameter, (b) bending curvatures due to mis-handling are easy to introduce, (c) microscopic observation of compressive failure is not always easy to make, when dealing with opaque materials such as carbon fibres, and (d) in the case of brittle fracture, it is impossible to determine the location of failure and whether it occurred on the tensile outer or compressive inner side of the fibre.

Axial compression tests on fibres are normally performed by embedding single fibres in a polymer matrix and by, subsequently, compressing the specimens parallel to the fibre axis [4]. The earliest stages of fibre failure can be identified either with optical microscopy [4] or, more recently, with Raman spectroscopy [5], leading to estimates of the fibre axial compression strength. This test provides an estimate of the compressive strength of a fibre as supported by resin, and is useful, particularly, when interfacial phenomena and/or differential Poisson's ratio effects are investigated.

Single fibres encapsulated into matrices can also be compressed either by differential thermal shrinkage between fibre and matrix [6–8] or by matrix contraction during solvent casting [9, 10]. However, in both cases, a triaxial state of stress is applied on the fibre and, therefore, it is not surprising that the compressive strength values obtained do not always compare well with the results obtained by other techniques described earlier.

DeTeresa *et al.* [11] developed a new method for applying well-defined and uniform compressive strains to single filaments by bonding them to the compressive

*Author to whom all correspondence should be addressed.

0022–2461/90 $03.00 + .12

side of an elastic rectangular transparent polymer beam which was then loaded in either cantilever [11], or, three-point bending configurations [9]. The fibres were glued on to the bars by means of a thin acrylic film which, in turn, transmitted the load to the fibres and supported them against global (Euler) instabilities. Provided that no slippage takes place between the fibre and the bar, the compressive strain varies linearly along the length of the beam and is only a function of the position on the bar, as determined by the elastic beam theory. The fibres were examined in the compressed state by flexing the beam while making observations with an optical microscope. The critical compressive strain for first compressive failure, indicated by fibre kinking or microbuckling, was determined by simply measuring the distance from the clamped end to the point where the last kink band was seen.

The cantilever beam type of test described above provides a quick and relatively easy way for measuring the compressive strain of high-performance fibres. In addition to that, measurements are conducted on the same continuous filament on which a stress gradient is applied and, hence, strain-gauge effects are, effectively, diminished. However, the applicability of this technique, as described by DeTeresa *et al.* [11], is restricted by the fact that optical microscopy was used to assess the compressive damage. As a result, the following drawbacks have, indeed, been noted [11]: (a) compressive failure could be detected only if a kink boundary was optically observed, (b) the amount of film shrinkage and/or residual load in the fibre could not be quantified, and (c) measurements on PAN-based carbon fibres could not be carried out due to the difficulty in assessing compressive damage in opaque fibres exhibiting rough surfaces.

In this programme of work, a modified version of the cantilever beam technique [11] was employed to compress the fibres axially, while the applied load in the fibre was measured by scanning along the length of the carbon filaments with the 2 μm probe of a laser Raman microscope. To our knowledge, this is the first time that the dependence of Raman vibrational frequencies of carbon fibres upon axial compression was investigated. Past work in this area [12] has shown that laser Raman spectroscopy (LRS) can be used to measure the response of a carbon fibre to applied tensile load at the molecular level. Certain relationships between Raman frequencies and applied tensile strain have been obtained for all the carbon fibre Raman bands [12] and this is of extreme importance in composite applications, because it is now possible to monitor the load that the reinforcing fibres experience by simply measuring their Raman frequencies.

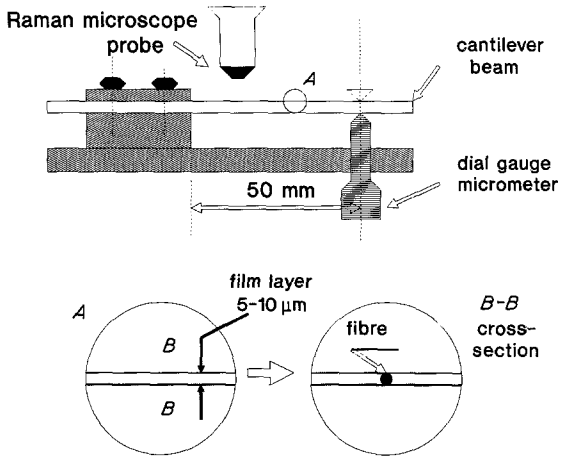

Figure 1 Schematic illustration of the cantilever rig assembly.

2. Experimental details

2.1. Samples and sample preparation

Four PAN-based carbon fibres of different moduli have been tested in this programme. The tensile mechanical properties of all the fibres are given in Table I.

The test specimens were prepared by aligning the single carbon filaments parallel to the length of PMMA bars and approximately at the centre of their width as shown in Fig. 1. The thickness and the width of the beams were kept fixed at 5.5 $\pm$ 0.1 mm and 10.0 $\pm$ 0.1 mm, respectively. The free length of the beams was kept normally fixed at 50 mm. The fibres were bonded to the bars by spraying them with a thin clear acrylic (Krylon) adhesive. Care was taken to keep the thickness of the adhesive down to 10 μm so its effect on the elastic beam calculations is insignificant. The film was dried for several hours in a vacuum oven at room temperature.

2.2. Cantilever rig

The design of the cantilever rig is shown in Fig. 1. The beam can be flexed up or down by means of a specially designed flat screw, subjecting the fibre to compression or tension, respectively. The fibres under load were examined with a laser Raman microscope which was located above the flexed beam, as shown in Fig. 1.

When the beam is flexed the maximum deflection, δ_{max}, of the neutral axis of the beam at the point of application of load is given by [13]

$$\delta_{max} = \frac{PL^3}{3EI} \quad (2)$$

where P is the applied load, L is the free length of the beam (Fig. 2), E the modulus and I is the moment of inertia. The moment, M, at any position x on the

TABLE I Tensile properties of PAN-based carbon fibres. The values have been obtained from the manufacturers. All Courtaulds Grafil fibres were unsized

Fibre	Manufacturer	Young's modulus (GPa)	Tensile strength (GPa)	Diameter (μm)
HM-st.	Courtaulds Grafil	390*	3.2	6.9
IM 43-750	Courtaulds Grafil	305*	5.5	5.0
XA	Courtlauds Grafil	230*	3.5	7.0
HMS4	Hercules	345	3.5	7.0

*Initial modulus values obtained by loading impregrated tows up to 0.4% strain.

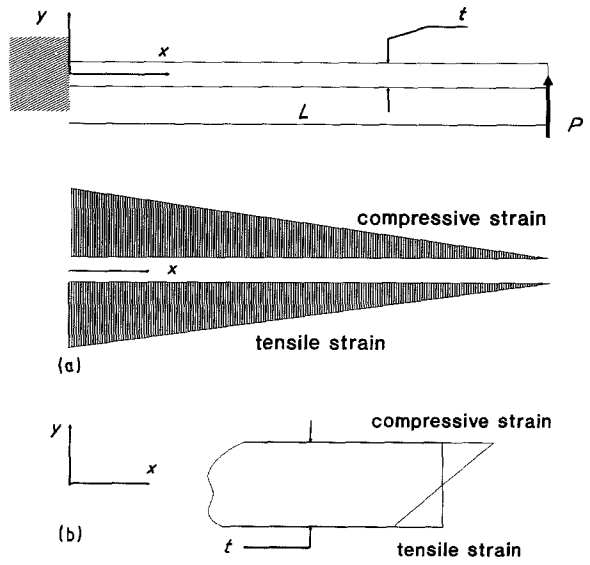

Figure 2 Distribution of (a) moment along the length, x, of the beam, and (b) axial compressive and tensile strains across the thickness, y, of the beam.

beam is given by

$$M = PL\left(1 - \frac{x}{L}\right) \quad (3)$$

The strain, ε, at positions x along the fibre and y away from the neutral axis (Fig. 2) is given by

$$\varepsilon_{(x,y)} = \frac{My}{EI} \quad (4)$$

Finally, the maximum strain on the outer surface of the beam can be found by substituting Equations 2 and 3 into Equation 4, and by setting y equal to half the thickness, t, of the beam (Fig. 2)

$$\varepsilon_{(x)}^{\max} = \frac{3t\delta_{\max}}{2L^2}\left(1 - \frac{x}{L}\right) \quad (5)$$

The distribution of strain on the fibre varies linearly with fibre length as can be seen from Equation 5 and Fig. 2. The distribution of load along the thickness of the beam is also shown in Fig. 2. Equations 2 to 5 are valid only if the PMMA grade used (ICIs "Perspex") exhibits identical tensile and compressive moduli and it does not creep significantly within the range of applied loads and the time required for testing. Extensive mechanical testing on our PMMA bars has shown that both conditions are satisfied up to a maximum strain of 1.5 to 1.6%.

In an attempt to assess the validity of the cantilever beam method, single carbon fibre filaments have also been mechanically loaded in tension in the air. A specially designed micro-extensometer mounted on the Raman microscope stage was employed, as described in a previous publication [12]. Both sets of tensile testing data are presented in Section 3 (Table II).

TABLE II Strain dependence of the Raman frequencies of the E_{2g} band of PAN-based carbon fibres upon tensile loading

Fibre	RFGF (micro-extens) (cm^{-1}/%)	RFGF (cantilever) (cm^{-1}/%)
HM-st.	-11.4 ± 0.2	-11.7 ± 0.3
IM 43-750	-7.0 ± 0.4	-6.9 ± 0.4
XA	-8.0 ± 0.5	-7.6 ± 0.4
HMS4	-10.5 ± 0.3	-10.4 ± 0.3

2.3. Raman spectroscopy

Raman spectra were taken with the 514.5 nm line of an argon ion laser. A modified Nikon microscope was used to focus the incident laser beam to a 2 μm spot on the fibre. Care was taken not to exceed a maximum laser power of 2 mW on the sample to avoid local overheating of the fibre/acrylic film system. The 180° backscattered light was collected by the microscope objective and focused on the entrance slit of a SPEX 1877 triple monochromator. A Wright Instruments charge-coupled device (CCD), cooled by liquid nitrogen, was employed as a photon counting system for recording of the Raman spectra. All the Raman frequency values reported in Section 3 were derived by fitting Lorentzian routines to the CCD raw data.

3. Results

The Raman spectra in the first-order region (540 to 570 nm) for all the fibres tested in this programme are given in Fig. 3. Two prominent bands are observed at 1360 and 1580 cm^{-1} corresponding to A_{1g} and E_{2g} vibrational modes, respectively [12, 14]. The ratio of the intensities of the two bands has been associated with graphitic crystallite size on the carbon fibre surface [14]. Indeed, as can be seen from Fig. 3, a gradual decrease of the A_{1g}/E_{2g} intensity ratio is obtained with decreasing modulus. A more detailed account of the effect of crystallinity/modulus upon the Raman spectra will be presented in a future publication [15].

All the different types of carbon fibres were tested both in tension and compression on the cantilever rig (Fig. 1) and the dependence of the Raman frequencies of the E_{2g} band (Fig. 3) upon tensile or compressive strain was examined. A typical Raman frequency–tensile strain curve is shown in Fig. 4a. The "frequency shift" in this and following graphs represents the difference between the Raman frequency values of the loaded part of the fibre and the values of the corresponding stress-free fibre in the air. As can be seen, a linear relationship is obtained within the experimental error all the way up to fracture. In the vicinity of the crack, the frequency drops gradually due to film failure and takes up its zero strain value at 1.0% applied tensile strain, where the crack is actually located. In Fig. 4b the relationship of frequency to tensile strain is plotted for the same type of fibre loaded in air by means of a micro-extensometer. Again, a similar type of trend is obtained up to a fracture strain of 0.9%.

The slopes of the linear relationships between Raman frequency and tensile strain up to approximately 1% strain, as derived from the cantilever beam and the micro-extensometer type of tests, are given in Table II. The values of these slopes, which, in fact, represent the Raman-frequency-gauge-factors (RFGF) in tension, were calculated by least-square-fitting to the experimental data. It can be seen that, within experimental error, similar values were obtained from

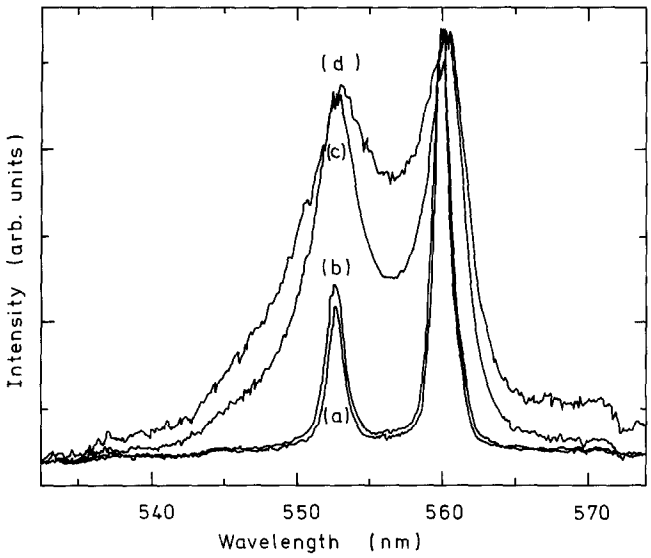

Figure 3 Raman spectra in the first-order region for the following fibres: (a) Courtaulds Grafil HM-Standard; (b) Hercules HMS4; (c) Courtaulds Grafil IM 43-750; and (d) Courtaulds Grafil XA. The Raman bands have been normalized to the intensity of the E_{2g} band.

the two different tests. Hence, the validity of both the cantilever beam method for axial loading of fibres and of Equation 5, are independently verified.

For cantilever compression testing, the Raman frequencies of all the embedded carbon fibres were recorded prior to loading and specimens found to exhibit Raman frequency values different from the values of the stress-free fibre in air, were discarded. Consequently, any fibres that contained residual stresses due to either film shrinkage and/or mishandling were not included in the measurements.

In Fig. 5 the Raman frequency shift, as defined above, is plotted as a function of compressive strain for a Courtaulds Grafil HM fibre. As expected, the Raman frequencies shift linearly to higher values with compressive strain up to the first compressive failure. The latter is indicated by the sudden drop of Raman frequencies at about 0.45% applied compressive strain. Microscopic examination of this region, revealed that the drop in Raman frequencies corresponds to the presence of a compression crack, as shown in Fig. 6b. It is interesting to note that the frequency picks up again after the first crack and becomes maximum at about 0.7% applied strain. This is then followed by further frequency drops at the second and subsequent cracks (Fig. 5). Experiments

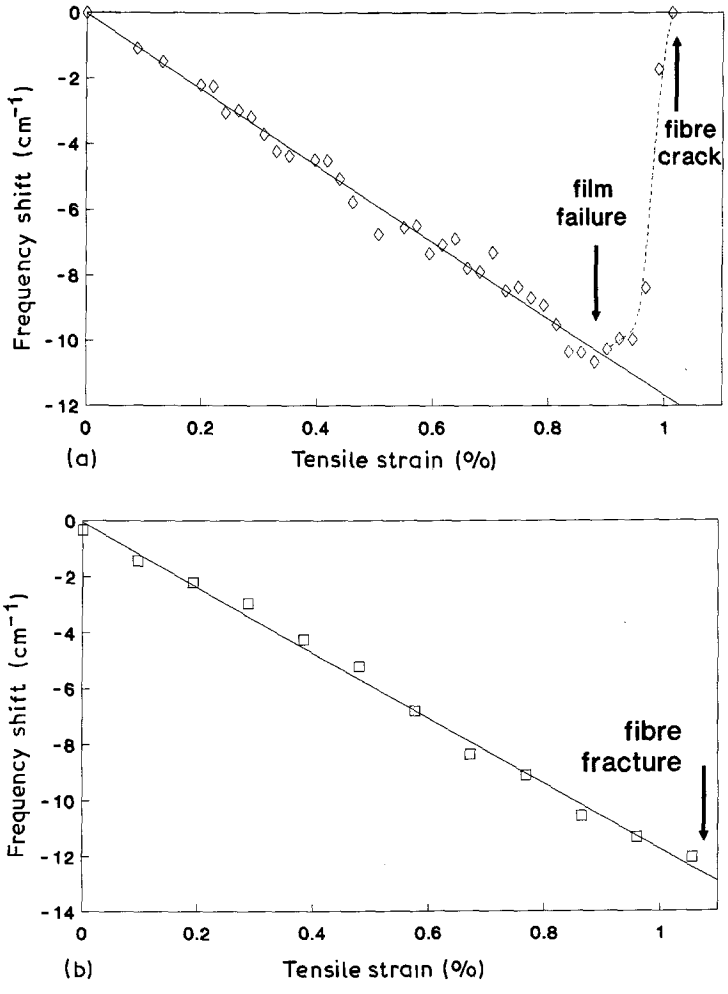

Figure 4 (a) Raman frequency shift of the E_{2g} band as a function of strain for a Courtaulds Grafil HM Standard fibre tested in tension on the cantilever beam. The values of strain along the fibre have been calculated from Equation 5. (b) Raman frequency shift as a function of strain for the same fibre loaded in the air by means of a micro-extensometer.

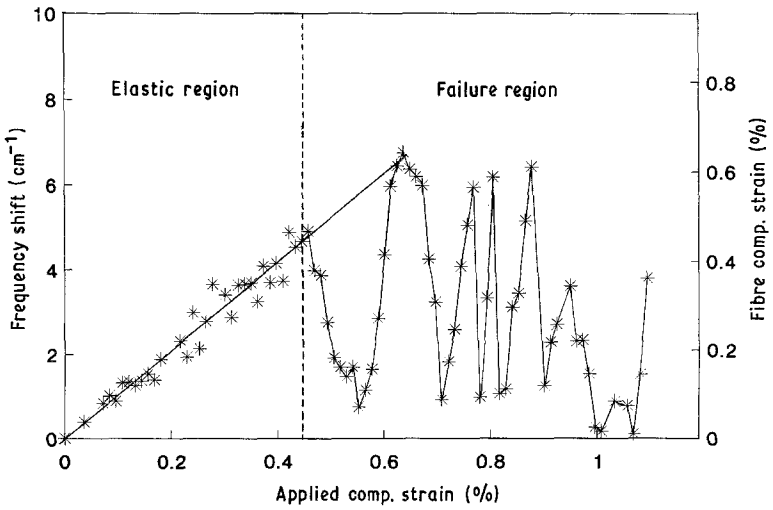

Figure 5 Raman frequency shift as a function of compressive strain for a Courtaulds Grafil HM fibre. Successive data points in the failure region have been interpolated.

performed on other PAN-based high-modulus fibres, such as HMS4 (Hercules), have demonstrated that compressive failure by transverse fibre cracking is the typical mode of compressive failure for these fibres. The values of critical compressive strain for both Courtaulds Grafil HM-standard and Hercules HMS4 are given in Table III.

The relationship between Raman frequency shift and compressive strain for Courtaulds Grafil IM 43-750 fibres is given in Fig. 7. The frequency shift appears to relate linearly to compressive strain up to a certain load, and then forms a plateau. The onset of this plateau is not well-defined, ranging from approximately 0.75% to 0.85% compressive strain. The appearance of the plateau and the considerable increase in the scatter of the frequency values beyond that point, strongly indicate the onset of compressive failure. Indeed, microscopic observations (Fig. 8b) confirmed that failure in the form of bulging was, indeed, present in that region (Fig. 8c).

In the case of low-modulus Courtaulds Grafil XA fibres two distinct types of behaviour were noticed, as half of the samples failed at approximately 0.9% applied strain, whereas the other half showed no signs of failure up to strains approaching the tensile fracture strain. In Fig. 9 the frequency–compressive strain curve is plotted for the "weak" type of fibres. It can be seen that, up to 0.9% applied compressive strain, a linear relationship between Raman frequency and compressive strain was obtained with no obvious signs of failure. At that point, the frequency dropped dramatically to the value of the stress-free fibre, and further frequency drops were observed at higher strains (Fig. 9). This effect was statistically variable as other fibres showed no compressive failure up to applied strains of about 1.5 to 1.6%, as can be seen in Fig. 10. The onset of the non-linear behaviour observed above 1.2% strain is thought to be associated with significant reduction in the compressive modulus at such high strains. Further loading to strains higher than 1.6% was not attempted due to the plastic deformation and creep of the Perspex bars, as mentioned earlier. Indeed, microscopic examination of the fibres at various levels of loading, confirmed that (a) the drop of frequency at 0.9% corresponds to failure in the form of bulging (Fig. 11), possibly initiated by the presence of a gross defect at that location, and (b) for the fibres of Fig. 10, no sign of compressive failure was detected up to strains as high as 1.5% to 1.6%.

The values of the slopes of the least-square-fitted straight lines up to first failure (Figs 5, 7, 9 and 10) are

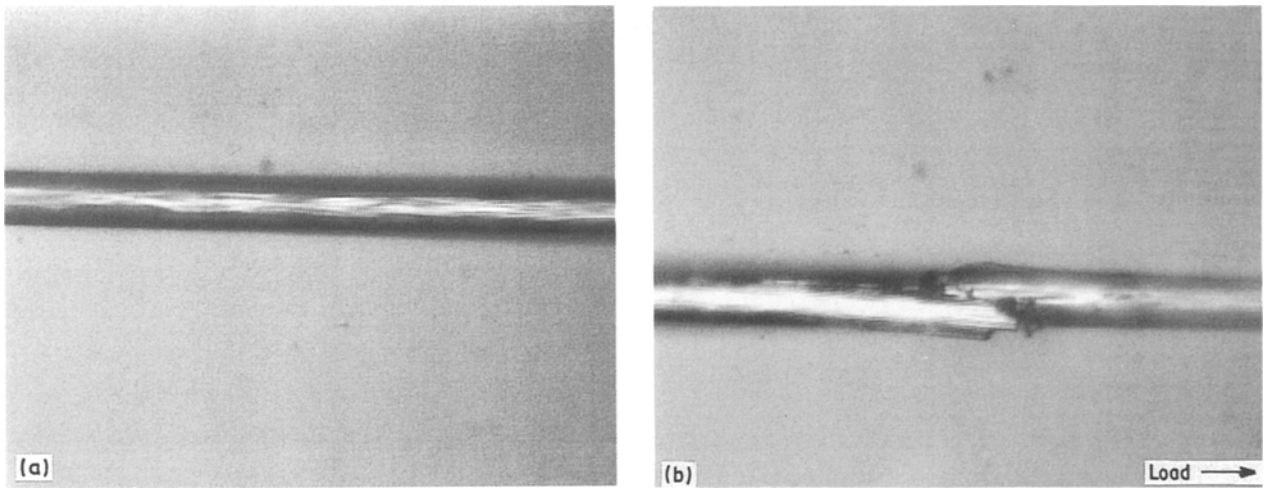

Figure 6 Reflection optical micrograph of a Courtaulds Grafil HM-standard fibre: (a) stress-free fibre; (b) at ~0.45% applied strain. The applied compressive strain increases in magnitude from left to right. The diameter of the fibre is 6.9 μm.

TABLE III Critical compressive strain to failure and dependence of the Raman frequencies of the E_{2g} band of PAN-based carbon fibres upon compressive loading up to first failure

Fibre	Critical compressive strain (%)	RFGF (cm^{-1}/%)	No. of fibres tested
HM-st.	0.45 ± 0.05	10.5 ± 0.7	4
IM 43-750	0.80 ± 0.10	4.7 ± 0.3	6
XA	⩾0.9	5.1 ± 0.3	4
HMS4	0.50 ± 0.05	10.1 ± 0.8	3

given in Table III. These RFGF values represent the strain dependence of Raman frequencies in the elastic region and can, in effect, be used as gauge factors in composite applications. By comparing the RFGF values of Tables II and III, two observations can be made: (a) the values in compression are consistently lower than the values in tension, and (b) the gap between the two sets of values appears to widen as the fibre tensile modulus decreases. The significance of these results is discussed below.

4. Discussion

4.1. Compressive modulus of carbon fibres

When fully crystalline fibres, such as polydiacetylene fibres (PDA) [16], are stressed, the macroscopic strain of the sample is equal to the microscopic strain at the atomic level. All the stress applied to the sample goes into stretching or compressing atomic bonds, hence, increasing or decreasing the bond length, respectively. The Raman vibrational frequencies related to these bonds will also change, shifting to lower values in tension [17] and to higher values in compression [18], as the interatomic distance increases or decreases, respectively. In fact, it has already been demonstrated by Fan and Hsu [18] that the RFGF, and also the elastic moduli for PDA fibres, have identical values in both tension and compression.

In partially crystalline fibres, such as carbon or aramid, not all the load applied to a specimen is effective in changing the interatomic separations, as part of that load is consumed for crystallite rotation, shear, etc. Thus, the RFGF values measured for carbon [12] or aramid fibres [19] depend upon the degree of crystallinity, much in the same way as the modulus, and express the effectiveness of the applied load in actually extending or contracting the atomic bonds. For example, in the case of aramid fibres of different moduli, it has already been demonstrated [20] that the RFGF values in tension are directly proportional to the tensile modulus. In Fig. 12, the RFGF values in tension for the carbon fibres examined here, are plotted as a function of tensile modulus (manufacturers' quoted values). Although at this stage of the project an insufficient number of fibres has been tested, it can be seen that the values for the Courtaulds Grafil HM-standard and XA fibres, as well as, for Hercules HMS4 fibre lie on a straight line which goes through the origin. The value for Courtaulds Grafil IM appears to deviate slightly from the linear trend. This discrepancy is attributed to its size, 5 μm diameter as opposed to 7 μm for the other carbon fibres (Table I), and, in particular, to structural changes that this reduction in size might have brought about. It is interesting to note here, that the slope of the straight line of Fig. 12 is $-2.8\,cm^{-1}\,GPa^{-1}$, whereas a value of $-3.6\,cm^{-1}\,GPa^{-1}$ was obtained from a series of aramid fibres of different moduli [21]. This difference in value reflects differences in the structure of the fibre and in the type of benzene-ring vibrational mode considered in each case [21].

Based on the above analysis, the RFGF values in tension or compression of partially crystalline fibres are, indeed, directly related to the initial tensile or compressive moduli, E^t or E^c, respectively. In mathematical terms

$$(\mathrm{RFGF})^{\mathrm{tension}} = kE^t \quad (6)$$

and

$$(\mathrm{RFGF})^{\mathrm{compression}} = kE^c \quad (7)$$

For PAN-based carbon fibres, the constant k is related only to the atomic vibrational mode (E_{2g} for both sets of data). Hence from Equation 6

$$E^c = \frac{(\mathrm{RFGF})^{\mathrm{compression}}}{(\mathrm{RFGF})^{\mathrm{tension}}} E^t \quad (8)$$

Equation 8 expresses the fact that the observed decrease of the RFGF values in compression with regards to the RFGF values in tension (Table III), corresponds to an equal reduction in the values of modulus for each individual fibre. In Table IV, the moduli calculated from Equation 8 are listed. It can be seen that the compressive moduli of highly crystalline HM fibres are reduced up to a maximum of 10% with

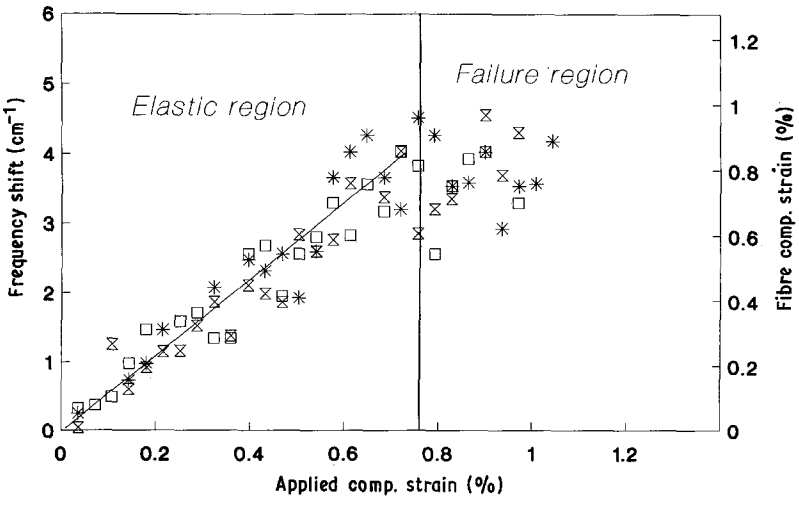

Figure 7 Raman frequency shift as a function of compressive strain for three different Courtaulds Grafil IM 43-750 fibres.

TABLE IV Ratio of the RFGF values in tension and compression and estimated compressive moduli and strengths for PAN-based carbon fibres

Fibre	$\frac{(RFGF)^{comp.}}{(RFGF)^{tens.}}$	E_c (GPa)
HM-st.	0.90 ± 0.08	351 ± 30
IM 43-750	0.68 ± 0.08	208 ± 25
XA	0.68 ± 0.07	154 ± 15
HMS4	0.96 ± 0.08	331 ± 25

respect to their tensile moduli, whereas reductions of approximately 30% are observed in the case of IM and XA fibres. Another way of estimating E^c is to solve Equation 8 as for E^c, setting k equal to $2.8\,cm^{-1}\,GPa^{-1}$, which is the value of the slope of Fig. 12. However, this route is less accurate in view of the insufficient number of data of Fig. 12 and the differences in size between the fibres.

To summarize, the RFGF values for 100% crystalline fibres, such as polydiacetylenes, are equal in tension [17, 18] and compression [18] and no variation of RFGF with modulus is observed. However, for partially crystalline fibres such as carbon or aramid the compressive modulus decreases with respect to the tensile modulus by an amount equal to the ratio of the RFGF values in compression and tension, respectively. In other words, the Raman data show that the applied load is less effective for contracting the bonds in compression than it is for extending the bonds in tension. Indeed, if the fibre is regarded as a chain of crystallites, each having a slight misorientation with respect to the fibre axis, then the application of a tensile load will tend to align the crystallites to the loading direction, whereas the application of compressive load will tend to align the crystallites normal to the loading direction. Hence, both initial and secant compressive modulus values should show a marked decrease with respect to corresponding values in tension. The presence of voids, pits etc. in the structure of carbon fibres should also make the material apparently softer in compression. In fact, early experimental evidence has been produced, by Curtis *et al.* [22] for the strain-hardening effect during tensile loading of carbon fibres, whereas more recent work [23] has indicated that the reverse strain-softening effect should be present during compressive loading. Furthermore, the results presented in Fig. 10 indicate that this effect is indeed quite pronounced for XA fibres, sufficient to alter the response of the Raman frequency with strain above 1.2% compressive strain. For kevlar 49 and poly-paraphenylene-benzobisthiazole (PBT) unidirectional composites, existing experimental evidence [24] agrees well with these findings.

4.2. Critical strain to failure

As mentioned earlier, the Raman technique presented here consists of an excellent method for measuring the critical compressive strain to failure of opaque materials such as carbon fibres. In Fig. 13 the critical compressive strain to failure is plotted as a function of the estimated Young's modulus in compression. It can be seen that the critical strain to failure decreases dramatically with increasing modulus within the 150 to 350 GPa range of moduli. However, due to the non-linearity of the stress–strain curves for tension [22] and compression [23], critical compressive stresses to failure are hard to estimate. In a future publication an attempt will be made to combine these data with extensive mechanical testing of unidirectional composites in both tension and compression.

It has already been reported that two competing factors determine the compressive strength of a PAN-based carbon fibre; the preferred orientation about the fibre axis [4, 25], and the shear modulus [25]. Indeed, with increasing axial modulus, the microfibrillar graphite ribbons of a carbon fibre tend to align themselves with respect to the fibre axis, but this beneficial effect is, in fact, cancelled out by the decrease of shear modulus as fibre anisotropy increases, leading to transverse cracking at relatively low applied compressive loads. Nevertheless, any attempt to model the compressive behaviour of PAN-based carbon fibres encounters many difficulties, due to complications arising from either the "onion skin" structure [26] of the fibres, or from gross imperfections, such as voids, flaws, surface pits etc. [27], which can affect the onset of compressive failure, particularly, of low modulus fibres.

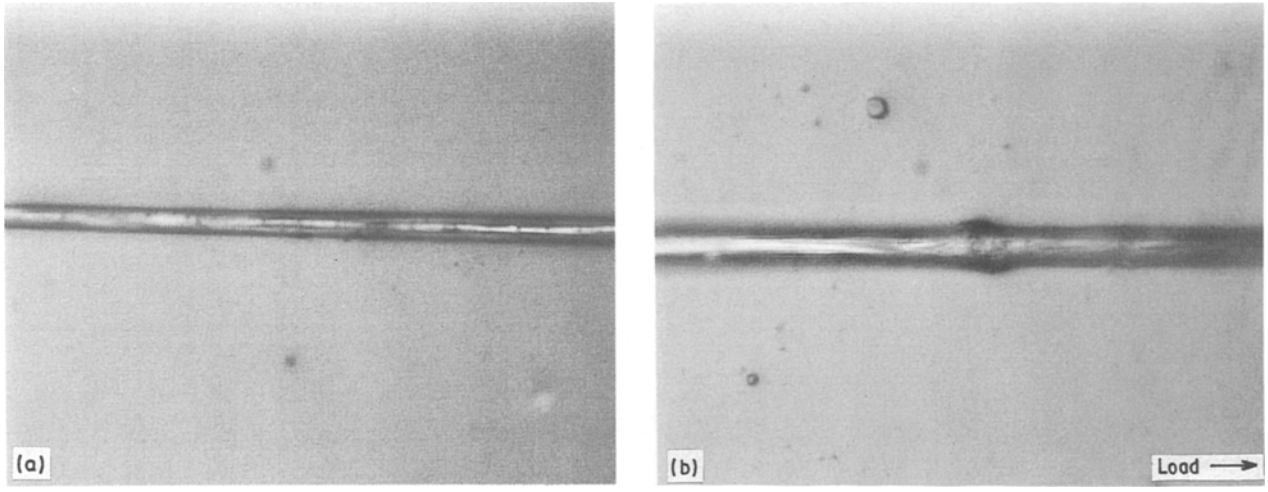

Figure 8 Reflection optical micrograph of a Courtaulds Grafil IM 43-750 fibre: (a) stress-free; (b) at ~0.8% applied strain. The applied compressive strain increases in magnitude from left to right. The diameter of the fibre is 5 μm.

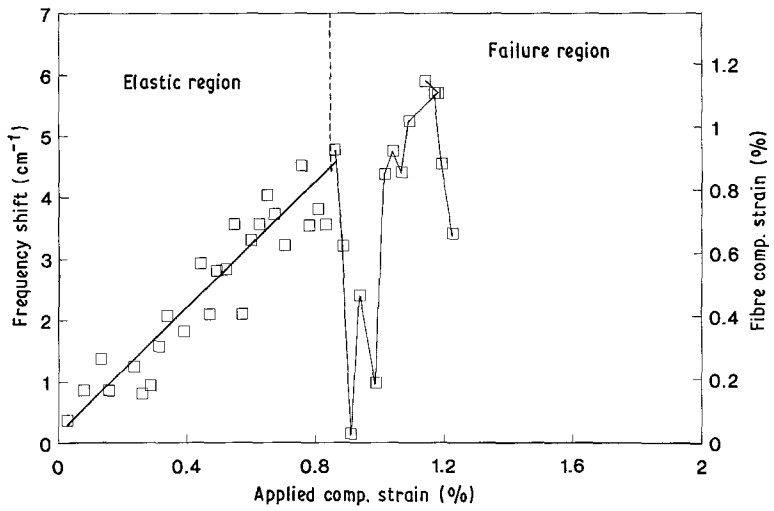

Figure 9 Raman frequency shift as a function of compressive strain for a Courtaulds Grafil XA fibre ("weak" type). Successive data points in the failure region have been interpolated.

4.3. Mechanisms of compressive failure/ residual load

4.3.1. High-modulus fibres

In general, high modulus fibres, such as HM-standard and HMS4, fail in compression by transverse cracking, as shown in Fig. 6b. Because a linear relationship between frequency and applied compressive strain has been established, the "frequency shift" axis can be converted for clarity to "fibre strain" in compression, as shown in Fig. 5. An examination of the strain that the fibre experiences in the "failure region" shows that the failure is, indeed, brittle with the load dropping to zero at each crack. It is interesting to note that after first failure/cracking, the strain in the fibre recovers at about 0.6% of the applied strain, as can be seen by extrapolating the least-square-fitted straight line of the "elastic region" (Fig. 5) to that value. However, as the density of the cracks increases, due to the stress gradient applied to the fibre, the length of each fibre fragment between successive cracks decreases. Therefore, from first failure onwards, the applied maximum compressive strain in the middle of each fragment lags behind the applied compressive strain in a somewhat diminishing fashion. This behaviour is reminiscent of the "fragmentation" test [28] and indicates that the same load-transfer mechanism operates both in tension and compression.

4.3.2. Intermediate modulus fibres

A different type of compressive failure is observed in IM fibres. When compressive failure by bulging (Fig. 8b) occurs, at ~0.8% strain (Fig. 8), a slight drop in the strain in the fibre is observed. At 1% applied strain, the fibre still supports between 0.6% and 1% strain. This indicates that some form of yielding (possibly due to contained microbuckling) is the failure mechanism in this case.

4.3.3. Low modulus fibres (XA)

The behaviour of the "weak" type of XA fibre in Fig. 9 is mainly attributed to the presence of structural defects. This view is further strengthened by the fact that bulging in this case is accompanied by fracture, as demonstrated by the dramatic drop in the frequency and, therefore, of the fibre strain to zero (Fig. 9). On the contrary, other XA fibres from the same batch deform elastically up to 1.2% applied compressive strain (Fig. 10), while no obvious signs of failure are observed up to strains as high as 1.5% to 1.6%. This variability in the compressive behaviour of the XA fibres (Figs 9 and 10) is not surprising in view of the low crystallinity and the high density of flaws that low modulus fibres contain.

The amount of the residual load that individual IM and, in some cases, XA fibres can sustain after failure

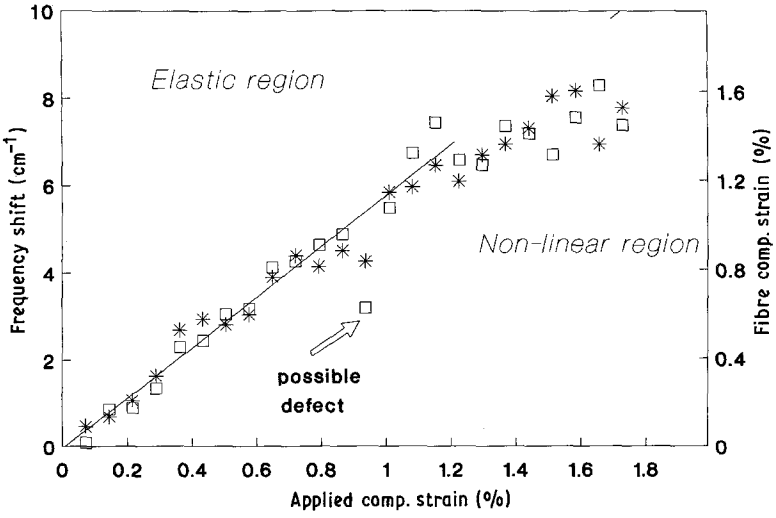

Figure 10 Raman frequency shift as a function of compressive strain for two different Courtaulds Grafil XA fibres ("strong" type).

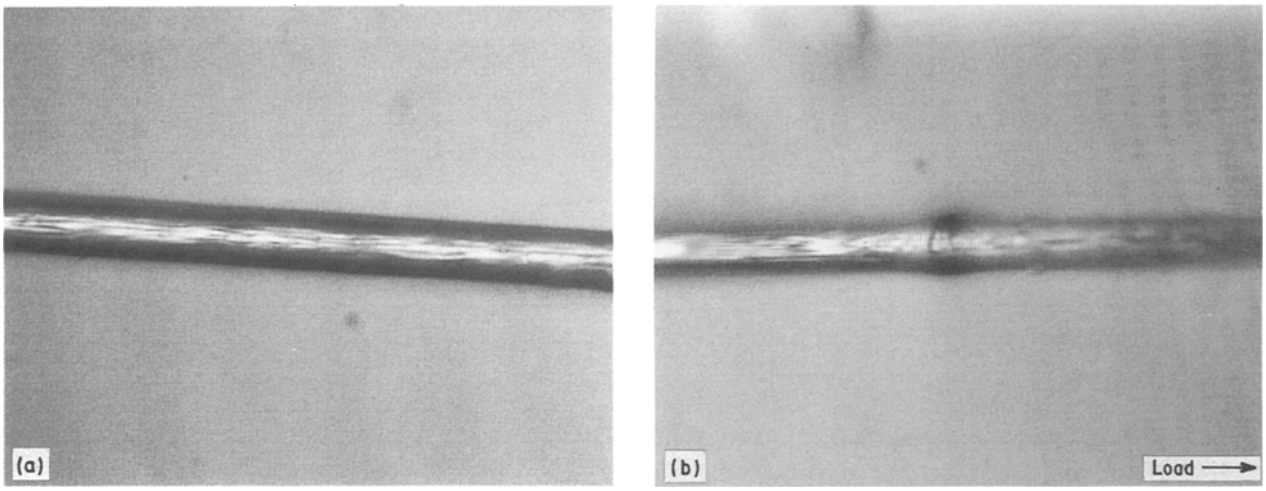

Figure 11 Reflection optical micrograph of a Courtaulds Grafil XA fibre: (a) stress-free; (b) at ~0.9% applied strain. The applied compressive strain increases in magnitude from left to right. The diameter of the fibre is 7 μm.

is indeed remarkable. Indeed, it now becomes apparent that the onset of compressive failure is not the only important parameter to be considered in this field, as other parameters such as the mode of failure and, in particular, the residual load that the fibre sustains after failure, can affect tremendously the mechanical and, in particular, the fatigue performance of carbon fibre composites.

4.4. Other applications of the cantilever beam/Raman technique

Carbon fibres fail in tension in a brittle manner and can fracture during mechanical testing into tiny fragments, causing nuisance and a serious health hazard to the operator. As mentioned in a previous section, the cantilever beam/Raman method can be used equally well in tension. In fact, the results already presented in Fig. 4 give a good example of such a test. For strain to failure measurements, the advantages of this test over conventional loading are the following:

1. The "gauge length effect" is eliminated by subjecting a very long fibre to a stress gradient.
2. Premature failure can be easily detected by the related frequency drop and the form of subsequent recovery.
3. The fibre is "frozen" in position and can be scanned several times.
4. The health hazard is prevented by encapsulating the fibre into a thin film.
5. The fibre can be easily recovered from the soluble

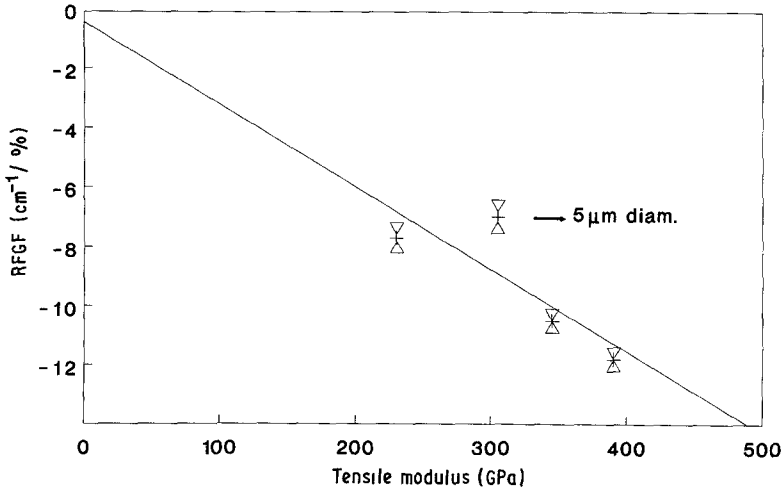

Figure 12 RFGF values in tension as a function of tensile modulus for PAN-based carbon fibres.

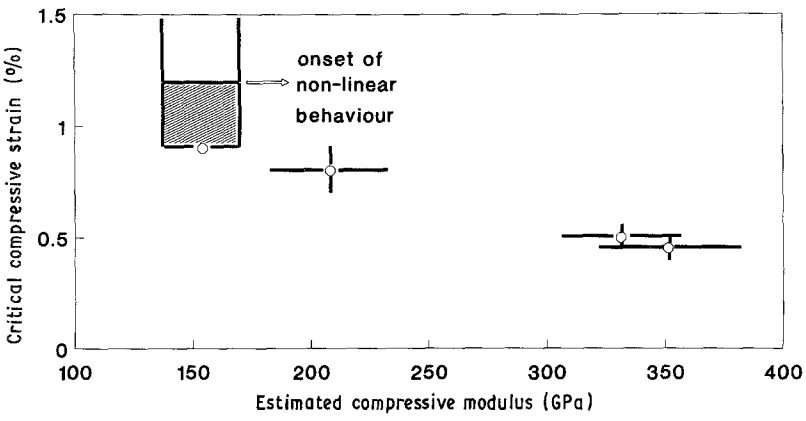

Figure 13 Critical compressive strain to failure as a function of estimated compressive Young's modulus for PAN-based carbon fibres.

film for subsequent investigations (SEM, fracture topography, etc.)

The application of the cantilever beam/Raman technique for tensile testing will be examined in depth in a future publication [29].

5. Conclusions

A new method for determining the critical compressive strain to failure and the compressive modulus of single PAN-based carbon fibres has been presented. This technique combines successfully a cantilever beam to load the fibres in tension or compression and Raman spectroscopy to map the strain along the fibres.

Experiments performed on a range of PAN-based fibres of different moduli have shown that (a) the elastic moduli in compression, particularly for intermediate (IM) and low modulus (XA) fibres, appear to decrease in value with regards to the initial tensile moduli, and (b) the critical compressive strain to failure increases as the modulus decreases for all the fibres tested.

Acknowledgements

This programme of research is funded by grants from the Royal Aerospace Establishment (MOD), the Department of Trade and Industry, Courtaulds Grafil plc, SERC and Queen Mary College, whose contribution is gratefully appreciated. We also, thank C.K.L. Davies, P. Tetlow, Department of Materials Queen Mary and Westfield College, and R. Robinson, S. Smith and J. Kirby, Courtaulds Grafil plc, for useful suggestions and assistance with the experiment.

References

1. D. SINCLAIR, *J. Appl. Phys.* **21** (1950) 380.
2. W. R. JONES and J. W. JOHNSON, *Carbon* **9** (1971) 645.
3. J. M. GREENWOOD and P. G. ROSE, *J. Mater. Sci.* **9** (1974) 1809.
4. H. M. HAWTHORNE and E. TEGHTSOONIAN, *ibid.* **10** (1975) 41.
5. H. JAHANKHANI and C. GALIOTIS, in "Interfaces in Polymer, Ceramic and Matrix Composites, edited by H. Ishida (Elsevier, New York, 1988) p. 107.
6. GILLHAM, P. N. REITZ and M. J. DOYLE, *Polym. Engng Sci.* **8** (1968) 277.
7. I. M. ROBINSON, P. H. J. YEUNG, C. GALIOTIS, R. J. YOUNG and D. N. BATCHELDER, *J. Mater. Sci.* **21** (1986) 3440.
8. I. M. ROBINSON, R. J. YOUNG, C. GALIOTIS and D. N. BATCHELDER, *ibid.* **22** (1987) 3642.
9. S. J. DeTERESA, S. R. ALLEN, R. J. FARRIS and R. S. PORTER, *ibid.* **19** (1984) 57.
10. W. C. DALE and E. BAER, *ibid.* **9** (1974) 369.
11. S. J. DeTERESA, R. S. PORTER and R. J. FARRIS, *ibid.* **23** (1988) 1886.
12. C. GALIOTIS and D. N. BATCHELDER, *J. Mater. Sci. Lett.* **7** (1988) 545.
13. S. P. TIMOSHENKO and J. M. GERE, "Theory of Elastic Stability" (McGraw-Hill, New York, 1961).
14. F. TUINSTRA and J. L. KOENIG, *J. Comp. Mater.* **4** (1970) 492.
15. N. MELANITIS, P. TETLOW, C. GALIOTIS and C. K. L. DAVIES, to be published.
16. C. GALIOTIS, PhD thesis, University of London (1982).
17. C. GALIOTIS, R. J. YOUNG, P. H. J. YEUNG and D. N. BATCHELDER, *J. Mater. Sci.* **19** (1984) 3640.
18. C. F. FAN and S. L. HSU, *J. Polym. Sci. (B) Polym. Phys.* **27** (1989) 337.
19. C. GALIOTIS, I. M. ROBINSON, R. J. YOUNG, B. J. E. SMITH and D. N. BATCHELDER, *Poly. Commun.* **26** (1985) 354.
20. S. VAN DER ZWAAG, M. G. NORTHOLT, R. J. YOUNG, I. M. ROBINSON, C. GALIOTIS and D. N. BATCHELDER, *Polum. Commun.* **28** (1987) 276.
21. C. GALIOTIS, unpublished data.
22. G. J. CURTIS, J. M. MILNE and W. N. REYNOLDS, *Nature* **220** (1968) 1024.
23. P. HENRAT, in "Looking Ahead for Materials and Processes", edited by J. de Rossu, G. Briens and P. Lissac (Elsevier, Amsterdam, 1987) p. 389.
24. S. KUMAR, W. W. ADAMS and T. E. HELMINIAK, Proceedings of the American Society for Composites, First Technical Conference, Technomic, Lancaster, PA (1986) p. 8.
25. S. J. DeTERESA, R. S. PORTER and R. J. FARRIS, *J. Mater. Sci.* **20** (1985) 1645.
26. D. HULL, "Introduction of Composites" Cambridge Solid State Science Series (Cambridge University Press, 1981) p. 10.
27. I. L. KALNIN and H. JAGER, in "Carbon Fibres and Their Composites" edited by E. Fitzer (Springer-Verlag, Berlin, 1985) p. 62.
28. A. KELLY and W. R. D. TYSON, *Mech. Phys. Solids* **13** (1965) 329.
29. N. MELANITIS and C. GALIOTIS, to be published.

Received 1 July
and accepted 16 August 1989